# Adsorption of hydrogen sulphide on Metal-Organic Frameworks

Gutiérrez-Sevillano, J.J.; Martín-Calvo, A.; Dubbeldam, D.; Calero, S.; Hamad, S.

**DOI**
10.1039/c3ra41682h

**Publication date**
2013

**Document Version**
Final published version

**Published in**
RSC Advances

RSC Advances

RSC Publishing

PAPER

View Article Online
View Journal | View Issue



# Adsorption of hydrogen sulphide on Metal-Organic Frameworks†

Cite this: *RSC Advances*, 2013, **3**, 14737

Juan José Gutiérrez-Sevillano,[a] Ana Martín-Calvo,[a] David Dubbeldam,[b] Sofía Calero[a] and Said Hamad*[a]

Received 23rd January 2013,
Accepted 18th April 2013

DOI: 10.1039/c3ra41682h

**www.rsc.org/advances**

Three new sets of interatomic potentials to model hydrogen sulphide ($H_2S$) have been fitted. One of them is a 3-sites potential (which we named 3*S*) and the other two are 5-sites potentials (which we named 5S and 5Sd). The molecular dipole of the 3S and 5S potentials is 1.43 D, which is the value usually employed for $H_2S$ potentials, while the dipole of the 5Sd is the dipole measured experimentally for the $H_2S$ molecule, circa 0.974 D. The interatomic potentials parameters were obtained by fitting the experimental vapour-liquid equilibrium, vapour pressure and liquid density curves. The potential parameters fitted so far for $H_2S$ have been obtained applying long-range corrections to the Lennard–Jones energy. For that reason, when a cut and shift of the Lennard–Jones potentials is applied they do not yield the correct results. We employed a cut and shift of the Lennard–Jones potentials in the fitting procedure, which facilitates the use of the new potentials to model $H_2S$ adsorption on systems such as Metal-Organics Frameworks (MOFs). We have employed the newly developed potentials to study the adsorption of $H_2S$ on Cu-BTC, MIL-47 and IRMOF-1 and the results agree with the available electronic structures calculations. All calculations (both quantum and interatomic potential-based) predict that $H_2S$ does not bind to the Cu atoms in Cu-BTC.

## I. Introduction

Hydrogen sulphide ($H_2S$) is a gas with harmful effects on human health. The main anthropogenic sources of emissions of $H_2S$ are chemical industries, biogas production plants, and water treatment plants. Even when present in small concentrations, $H_2S$ can be detected by humans, so there are many efforts being made towards achieving methods of reducing as much as possible the amount of $H_2S$ present in the gases that are emitted by water treatment plants. Currently the two most frequently used methods for reducing the amounts of $H_2S$ emitted are biological treatments and chemical scrubbing.[1] But there is an increasing body of research[2–10] devoted to investigate the ability of different materials to adsorb $H_2S$. One set of studied materials is formed by Metal–Organic Frameworks[11,12] (MOFs), which have a wide range of properties in terms of adsorption, since they are structures with a variety of metal centres (Cu, Zn, Ti, *etc*), of pore sizes (large, medium or small) or even of framework flexibility.[13–15] In this study we will focus on the study of $H_2S$ adsorption on three well known MOFs, namely Cu-BTC, MIL-47, and IRMOF-1.[16–20] The main problem when trying to model $H_2S$ adsorption is that the choice of the interatomic potential parameters is of key importance. Despite the availability of a number of force field parameters,[21–28] they are often quite complex and their performance in modelling adsorption has not been tested extensively so far.

One problem in which we are particularly interested is the adsorption of $H_2S$ on Cu-BTC. There have been a number of experimental studies[9,29] which suggest that $H_2S$ molecules adsorb preferentially on the metallic centres and subsequently induce the decomposition of the framework. Although it has also been observed that the presence of water is crucial to the adsorption of $H_2S$,[30] simulation studies employing any of the existing force fields predict a different pattern of adsorption when $H_2S/H_2O$ mixtures are adsorbed in Cu-BTC. In a DFT study, Watanabe and Sholl[31] observed that the adsorption of $H_2O$ molecules on the metal centres of Cu-BTC is energetically favoured over the adsorption of $H_2S$ molecules. Employing Monte Carlo simulations to study the adsorption of various molecules in Cu-BTC, Castillo *et al.*[32] found that water has a surprisingly large affinity for the metal centre in Cu-BTC compared to other molecules such as carbon dioxide, nitrogen, oxygen or hydrocarbons. In a set of preliminary calculations Kristóf and Liszi[23] we found that indeed water molecules bind preferentially to the Cu atoms, while $H_2S$ molecules stay at the centre of the small cages of the structure.

[a]*Department of Physical, Chemical and Natural Systems, Universidad Pablo de Olavide, Ctra. Utrera, km. 1, 41013, Seville, Spain. E-mail: said@upo.es*
[b]*Van 't Hoff Institute for Molecular Sciences, University of Amsterdam, Science Park 904, 1098 XH Amsterdam, Netherlands*

† Electronic supplementary information (ESI) available: S1. Influence of the molecular dipole on the adsorption; S2. Variation of the average occupation profile with the molecular dipole; S3. Snapshots of *ab initio* Molecular Dynamics simulations of $H_2S$ and $H_2O$ adsorbed on a cluster model of Cu-BTC. See DOI: 10.1039/c3ra41682h

**Table 1** Interatomic potential parameters and the most relevant geometric information of all the sets of potentials parameters developed specifically for $H_2S$

| | Number of sites | $\varepsilon/k_B$ (K) S | $\sigma$ (Å) S | $q_S$ (e) | $q_H$ (e) | $q_A$ (e) | $\delta$ (Å) | $\delta'$ (Å) | $d_{S-H}$ (Å) | H–S–H angle (°) |
|---|---|---|---|---|---|---|---|---|---|---|
| Jorgensen *et al.*[28] | 3 | 125 | 3.7 | −0.47 | 0.235 | | | | 1.34 | 92 |
| Forester *et al.*[22] | 3 | 125 | 3.7 | −0.47 | 0.235 | | | | 1.3322 | 92.1 |
| | 4 | 269 | 3.69 | 0.661 | 0.278 | −1.217 | 0.1933 | | 1.3322 | 92.1 |
| | 5 | 163 | 3.69 | 0.614 | 0.145 | −0.452 | −0.0377 | 0.719 | 1.3322 | 92.1 |
| Kristóf and Liszi[23] | 4 | 269 | 3.69 | 0.661 | 0.278 | −1.217 | 0.1933 | | 1.34 | 92 |
| | 4 | 250 | 3.73 | 0.4 | 0.25 | −0.9 | 0.1862 | | 1.34 | 92 |
| Kamath *et al.*[26] | 3 | 278 | 3.71 | −0.252 | 0.126 | | | | 1.34 | 92.5 |
| | 3 | 252 | 3.72 | −0.338 | 0.169 | | | | 1.34 | 92.5 |
| | 3 | 232 | 3.72 | −0.380 | 0.19 | | | | 1.34 | 92.5 |
| | 3 | 219 | 3.72 | −0.4 | 0.2 | | | | 1.34 | 92.5 |
| Delhommelle *et al.*[24] | 5 | 230[a] | 3.74[a] | 1.393 | 0.323 | −2.039 | 0.1933 | | | |

[a] The Lennard–Jones centre is not the S atom, but a dummy site placed along the $C_2$ axis (which is the only rotation axis of the molecule) at a distance of 0.1254 Å from the S atoms towards the H atoms. $\delta$ is the distance, along the $C_2$ axis, between the sulphur atom and the additional charge. $\delta$' is the distance between the sulphur atom and the two additional charges, placed in a tetrahedral arrangement above and below the molecular plane.

All these results obtained from simulation studies are in apparent contradiction with the experimental observations, or with the way in which the experimental data are interpreted. We therefore set up to develop a new set of force field parameters in order to check whether a model that provides a dipole moment closer to the experimental one could predict an adsorption behavior more similar to the experimental one described. We have also studied the influence of the number of sites on the adsorption properties of $H_2S$, not only on Cu-BTC, but also on MIL-47 and IRMOF-1.

Achieving realistic modelling of $H_2S$ is a challenging task, which has been undertaken in several studies. In Table 1 we present the whole set of interatomic potentials parameters (or simply 'force field') which, to the best of our knowledge, have been published so far. Each force field has been fitted to model a particular aspect of the behaviour of $H_2S$. The first force field is that of Jorgensen,[28] who introduced some changes into the OPLS[21] force field (Optimized Potentials for Liquid Simulations) to model a range of liquid sulphur compounds, $H_2S$ among them. The force field is based upon a 3-site model of the $H_2S$ molecule, such as that shown in Fig. 1a. Its main finding regarding $H_2S$ is that there are no strong interactions between $H_2S$ molecules. The dimerisation energy pair distribution has a broad peak centred roughly around −1.0 kcal mol$^{-1}$, so that if the dimerisation energy cut-off employed to define a hydrogen bond is a reasonable value such as −2.25 kcal mol$^{-1}$, 92% of the molecules are monomers and the percentage of hydrogen bonded molecules is only 8% in the liquid phase. Jorgensen also calculated the radial distribution functions (RDFs) S–S and S–H, although at the time there were no experimental data for comparison.

As mentioned above, Jorgensen[28] employed a simple 3S model to describe the $H_2S$ molecule, with a negative charge at the S atom and positive charge at the H atoms. A better description of the electrostatic potential around $H_2S$ molecule could be achieved by increasing the complexity of the model, as it is usually done to simulate water molecules.[32,33] For instance, an additional charge can be placed on the $C_2$ axis of the molecule, at a distance $\delta$ from the sulphur atom, towards the hydrogen atoms, so that a 4S model is generated (see Fig. 1b). Similarly to $H_2O$ molecules, $H_2S$ molecules have two pairs of non-bonding electrons in non-occupied $sp^3$ orbitals of the S atom, thus the S atom is surrounded by four pairs of electrons arranged in a tetrahedral manner. In order to model this charge distribution a 5S model (see Fig. 1c) is often employed, which includes charges on the three atoms as well as in two additional sites placed above and below the $C_2$ axis, at a distance $\delta'$ from the sulphur atom.

Forester *et al.*[22] studied the three types of force fields for $H_2S$. The first one is the 3S force field developed by Jorgensen[28] with a slight change to the geometrical parameters. The second and third force fields are newly developed ones, with 4 and 5 sites respectively. All the parameters are shown in Table 1. They found that the 3S force field developed by Jorgensen[28] provides a poor description of $H_2S$ dimers. The force field that best agreed with the experimental data was the one employing a 4S model of the molecule. They validated

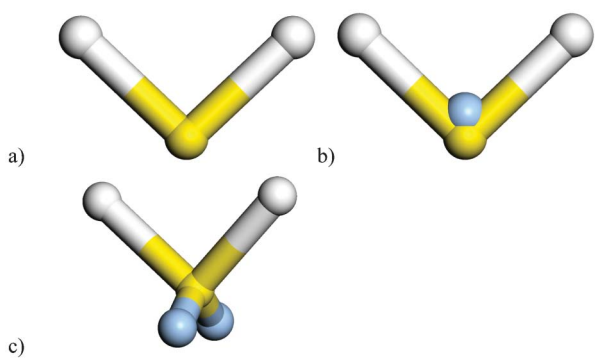


**Fig. 1** The three types of models which are commonly used for $H_2S$: a) three-site (3S), b) four-site (4S), c) five-site (5S). Yellow and white balls represent sulphur and hydrogen atoms respectively. Blue balls represent dummy sites where charges can be included.

 

their force fields by comparing the simulated RDFs with the experimental RDFs obtained by Andriani *et al.*[34] who performed XRD measurements of liquid $H_2S$. The three force fields predicted the first peak of the S–S RDF to be shifted inwards, while the second peak is correctly positioned. They also compared their simulation results with a range of dynamical properties of the liquid and high-temperature solid phases and found that the 4S force field was the one that yielded a better agreement with the experiments.

An important experimental set of data which was not included by Forester *et al.*[22] in the fitting of their interatomic potential parameters is the vapour–liquid equilibrium (VLE) curve of $H_2S$.[35] In a later study Kristóf and Liszi[23] employed a newly developed NpH Gibbs ensemble Monte Carlo simulation method[36] to carry out simulations of the coexistence of the liquid and vapour phases of $H_2S$ with which to parameterize a new force field. They studied three different force fields. The first one is the 3S force field developed by Jorgensen.[28] The second one is 4S force field developed by Forester *et al.*[22] (although with small differences in the intramolecular geometry). The third one is a re-parameterization of the latter, with the aim of providing a better agreement between the simulated and experimental VLE curves. Their new 4S force field achieved this goal and it also increased the agreement between the simulated and experimental S–S RDFs. Since we will refer often to the latter 4S force field we will refer to it as the KL force field.

The force fields described so far include the polarizability of the $H_2S$ molecule implicitly, through the presence of a permanent dipole due to the point charges distribution. There have been efforts to develop $H_2S$ models which take into account the polarizability, for example by using isotropic multipolar models[37] or Stockmayer potential models.[25] But these models perform marginally better, if at all, than simpler models, and their higher complexity limits their applicability, since these models are not implemented in all molecular simulation codes, are somewhat difficult to implement and introduce new problems regarding the combination rules. With the aim of including an explicit description of the polarizability of the $H_2S$ molecule, Delhommelle *et al.*[10] developed a new 5S force field, in which the atomic centres bore no Lennard–Jones interactions. A large negative charge was placed at an additional site a small distance from the S atom along the $C_2$ axis. The Lennard–Jones centre was placed at an additional polarizable, chargeless site located at a small distance along that axis. However, this additional complexity of the model does not bring a significant increase of the accuracy of the simulations of pure $H_2S$ phases, since the VLE curves are already well reproduced by the simpler force field developed by Kristóf and Liszi.[23] They found that it is important to consider explicitly the polarizability of $H_2S$ in order to obtain the correct mixing behavior of mixtures of species with very different dipoles, such as $H_2S$/n-pentane. But this was refuted by Kamath *et al.*,[26] who developed four simpler 3S force fields to model $H_2S$/n-pentane mixtures. They studied the influence of the atomic charges on the liquid phase behavior of $H_2S$, by studying four different charges for the S atom, namely −0.252 e, −0.338 e, −0.380 e and −0.400 e. The Lennard–Jones parameters were accordingly refitted to obtain a good description of the VLE curves. The RDFs and the liquid phase properties are well described by all parameters sets, although $H_2S$/n-pentane mixtures are better described by the two models with higher charges (charges of −0.380 e and −0.400 e for the S atoms). They stated that it is therefore possible to reproduce the phase behavior of complex mixtures including polar and non-polar components without recurring to use very complex models for the molecules; a careful fitting of the charges and Lennard–Jones potential parameters is enough in the case of $H_2S$/n-pentane mixtures. In a recent article Hellman *et al.*[27] developed a new force field, by fitting the interatomic potential parameters in order to reproduce a six-dimensional potential energy hypersurface for two rigid $H_2S$ molecules calculated with high level CCSD(T)/aug-cc-pV(Q + d)Z calculations. The force field provides very good predictions of the second pressure virial coefficient, shear viscosity and thermal conductivity, with results that are within the experimental error bars. This force field, however, is also a very complex one, since the functional form of the energy includes two damping functions and it makes use of 11 sites per molecule, with a total number of site-site interaction parameters of 140. It is therefore very complex to use this force field to study the interaction of $H_2S$ with other molecules.

Although all the force fields mentioned above provide an accurate description of liquid and gas phases of $H_2S$, they predict a weak interaction between $H_2S$ molecules and Cu atoms of the Cu-BTC framework, which contradicts previous

**Table 2** Interatomic potential parameters and values of the most relevant geometric information of the three $H_2S$ force fields developed in this study, as well as the other two existing force fields also employed

| Force field name | Number of sites | $\varepsilon/k_B$ (K) S | $\sigma$ (Å) S | $q_S$ (e) | $q_H$ (e) | $q_A$ (e) | $\delta$ (Å) | $d_{S-H}$ (Å) | H–S–H angle (°) |
|---|---|---|---|---|---|---|---|---|---|
| 3S | 3 | 275 | 3.7 | −0.32 | 0.16 | | | 1.34 | 92 |
| 5S | 5 | 295 | 3.75 | 0.0 | 0.152 | −0.152 | 0.3 | 1.34 | 92 |
| 5Sd[a] | 5 | 310 | 3.71 | 0.0 | 0.1027 | −0.1027 | 0.3 | 1.34 | 92 |
| KL[b] | 4 | 250 | 3.73 | 0.4 | 0.25 | −0.9 | 0.1862 | 1.34 | 92 |
| Kamath[c] | 3 | 232 | 3.72 | −0.38 | 0.19 | | | 1.34 | 92.5 |

[a] This force field has been fitted to model correctly the 0.974 D dipole of the $H_2S$ molecule. [b] This force field is the 4S force field developed by Kristóf and Liszi.[23] [c] This force field is the flexible 3S force field developed by Kamath *et al.*[26]

experimental observations. We therefore set to develop three new force fields with different number of interaction sites and dipole moments, in order to check whether they still predict the same adsorption patterns. In the present article we have studied the influence of the number of sites on the adsorption properties of $H_2S$ in Metal–Organic Frameworks, and we have developed new simple force fields able to provide a good description of the VLE curves. We also study the performance of these new force fields when describing the adsorption in the Metal–Organic Frameworks Cu-BTC, MIL-47, and IRMOF-1.

## II. Computational details

The adsorption isotherms were computed using Monte Carlo (MC) simulations in the $\mu$VT ensemble, where the chemical potential, volume and temperature were kept fixed. The MC moves were performed in cycles and in each cycle one of the following trial moves was selected at random for a given molecule: translation, rotation, reinsertion at a random position, insertion and deletion. Coulombic interactions were computed using the Ewald summation.

We studied the adsorption of $H_2S$ in Cu-BTC, IRMOF-1 and MIL-47 frameworks. The structures were modeled as rigid networks and the positions of the atoms were taken from Chui *et al.*[17](Cu-BTC), Eddaoudi *et al.*[38](IRMOF-1) and Barthelet *et al.*[20](MIL-47). The Lennard–Jones parameters for the structures were taken from the DREIDING[39] force field except those for Cu, V, and Cr, which were taken from the UFF[40] force field. We used Lorentz–Berthelot mixing rules to calculate mixed Lennard–Jones parameters. Atomic charges were taken from Frost and Snurr[41] and Dubbeldam *et al.*[42] for IRMOF-1, Castillo *et al.*[32] for Cu-BTC and from Bueno–Perez *et al.*[43] for MIL-47. Detailed information about the materials can be found elsewhere.[43–47]

The vapour-liquid equilibrium and vapour pressure curves are calculated by means of Monte Carlo simulations in the Gibbs ensemble.[48] Gibbs ensemble simulations are performed in two microscopic regions within the bulk phases, away from the interface. Each region is simulated within standard periodic boundary with a unit cell of $30 \times 30 \times 30$ Å.$^3$ The thermodynamic requirements for phase coexistence are that each region should be in internal equilibrium, and that the temperature, pressure, and chemical potentials of all components should be the same in the two regions. In order to achieve that we performed three types of Monte Carlo "moves", displacements of particles within each region (to satisfy internal equilibrium), fluctuations in the volume of the two regions (to satisfy equality of pressures) and transfers of particles between regions (to satisfy the equality of chemical potentials of all components). These moves were performed in cycles selecting one random move for each molecule in each cycle. The temperature, total number of particles, and total volume employed in the MC simulations were specified in advance and kept constant during the simulations. The simulations consisted on $10^5$ production cycles and $5 \times 10^4$ equilibration cycles. 166 $H_2S$ molecules were placed initially in each box to reproduce the experimental critical density of $H_2S$.

Classical MC simulations in the $\mu$VT and Gibbs ensembles were performed using the RASPA code.[49] This code developed by D. Dubbeldam, S. Calero, D. E. Ellis and R.Q. Snurr has been employed in several studies of gas adsorption.[49–52]

The electronic structure calculations were performed at DFT level, using the Gaussian09 code.[53] In order to take into account the presence of open metal centres and non covalent interactions at a reasonable computational cost we made use of Density Functional Theory calculations, with the hybrid *meta* exchange–correlation functional M06-2X, developed by Zhao and Truhlar.[54] which has been proven to provide reliable results for this type of systems at a reasonable computational cost.[55,56] The metal atoms were modelled with the Stuttgart/Dresden effective core potentials[57] and basis set, with 10 core electrons, while the 6–31++G** basis set for the rest of the atoms. The counterpoise method[58] was employed to reduce the basis set superposition error. In order to keep the cluster models as realistic models of the systems, we carried out the energy optimizations allowing the adsorbate molecules to relax, but keeping the atoms of the framework fixed at their experimental positions.

## III. Results and discussion

### A) Fitting of the new parameters to model experimental data

We have employed the experimental[59] data of the VLE curve to fit the interatomic potential parameters of the three new force fields. The first one is a 3-site force field, which we name as 3S. The second one is a 5-site force field which we name as 5S. Since one of the aims of this article is to study the influence of the number of sites on the adsorption properties, we kept the same dipole of the $H_2S$ molecule in these two force fields. In order to compare with the force field developed by Kristóf and Liszi[23], we have chosen the point charges in such a way that the dipole in the two new force fields is the same dipole than that of the KL force field, namely 1.43 D. This value is higher than the experimental value, which is 0.974 D.[60,61] The third force field we have developed is a 5-site potential with the correct value of the dipole moment. We will name this force field as 5Sd. For the sake of comparison, we have also calculated the VLE curve employing the Kamath *et al.*[26] force field (which we will refer to as Kamath). All parameters are listed in Table 2.

The VLE curves obtained with the 3*S*, 5S and 5Sd force fields are shown in Fig. 2, where the experimental curve and those predicted by the KL and Kamath force fields are also shown.

The three new force fields give an excellent agreement with the experimental curve, as is also the case of the previous ones, the KL and Kamath force fields. It is important to note that the newly developed force fields do not employ long-range corrections,[62] while they are employed in the previous ones. It has been suggested that simulations in which the Lennard–Jones potentials are cut and shifted could provide better results when modelling adsorption on crystalline confined

 

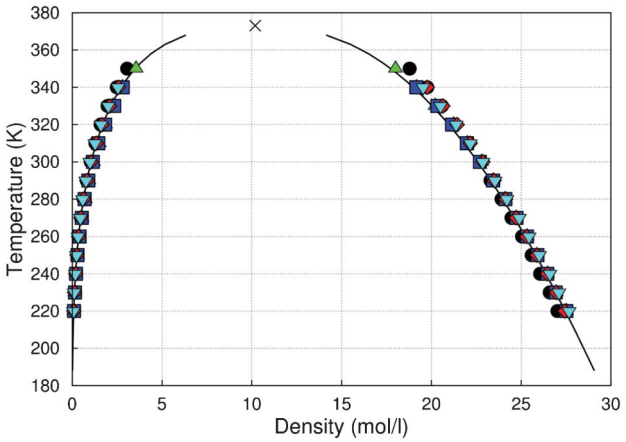


**Fig. 2** Comparison between the VLE experimental[59] curve (line) and those obtained with the three newly developed force fields, 3S (upwards pointing triangles), 5S (squares) and 5Sd (circles), and the force fields developed by Kristóf and Liszi[23] (diamonds) and Kamath *et al.*[26](downwards pointing triangles). The cross represents the critical point predicted from the experimental data.

**Table 3** Critical parameters obtained with experiment as with the KL, Kamath, 3S, 5S, and 5Sd force fields. The parameters were predicted using the density scaling law and the law of rectilinear diameters

| | *T*/K | Density (mol $l^{-1}$) | Pressure (MPa) | Beta |
|---|---|---|---|---|
| Experiment | 373.10 | 10.19 | 9.00 | |
| KL | 378.07 | 10.279 | 8.794 | 0.325 |
| | 375.42 | 10.337 | 8.624 | 0.315 |
| | 374.91 | 10.348 | 8.557 | 0.313 |
| Kamath | 375.78 | 10.169 | 8.858 | 0.325 |
| | 373.24 | 10.229 | 8.503 | 0.315 |
| | 371.2 | 10.278 | 8.227 | 0.307 |
| 3S | 381.62 | 10.242 | 9.347 | 0.325 |
| | 379.13 | 10.293 | 9.017 | 0.315 |
| | 376.14 | 10.354 | 8.632 | 0.303 |
| 5S | 371.57 | 10.285 | 8.919 | 0.325 |
| | 369.45 | 10.333 | 8.63 | 0.315 |
| | 367.2 | 10.387 | 8.319 | 0.304 |
| 5Sd | 371.83 | 10.829 | 9.601 | 0.325 |
| | 369.42 | 10.344 | 9.237 | 0.315 |
| | 366.33 | 10.415 | 8.783 | 0.302 |

systems than simulations in which conventional long-range corrections[63] are applied. Although long-range corrections can indeed be employed to model accurately adsorption on crystalline confined systems.[64] All the force fields to model $H_2S$ that have been published so far employ long-range corrections to the Lennard–Jones interaction. In order to provide the possibility to choose, we developed the new force fields employing a cut and shift of the Lennard–Jones potentials from 12 Å.

We obtained the parameters at the critical point, employing the density scaling law (1) and the law of rectilinear diameters[65–68] (2):

$$\rho_{liq} - \rho_{vap} = B\cdot(T - T_C)^{\beta} \quad (1)$$

$$(\rho_{liq} + \rho_{vap})/2 = \rho_C + A\cdot(T - T_C) \quad (2)$$

Due to the nature of these equations, the values of the critical temperature, density and pressure are very sensitive to the value of the $\beta$ parameter employed. In Table 3 we show the critical parameters obtained with different values of the $\beta$ parameter, 0.325 (the value employed by Kamath *et al.*[26]), 0.315 (the value employed by Kristóf and Liszi[23]) and the value obtained by letting the $\beta$ parameter vary in the fitting procedure. Given the large errors involved in this type of calculations, all force fields predict the critical parameters with a reasonable degree of accuracy.

We can get a further insight into the performance of the different force fields by analyzing the vapour pressure curve. Employing the interatomic parameters developed from the fitting of the VLE curve (which are shown in Table 1) we obtain the correct dependence of the vapour pressure *versus* temperature for all force fields studied, as can be seen in Fig. 3a. The deviation from the experimental data at low temperatures could also be analyzed by examining the plot of log P *versus* 1/T (see Fig. 3b).

The best results are lower temperatures are obtained with the KL force field, while the Kamath force field is the one that provides results further away from the experimental data. But the differences between all the force fields are not significant. In order to get a deeper insight into how each of the force fields performs in the whole range of temperature we also plot, in Fig. 3c, the absolute error between the calculated and experimental values of adsorption. We can see that the smaller error is obtained with the 3S and 5S force fields, followed by 5Sd and KL, which are very close to each other, while the Kamath force fields provides the largest errors. But again, the errors are all relatively small (typically less than 10%), so the comparison between the different force fields and the experimental data shown in the previous figures cannot be employed to assess which of them can model the system in a more realistic manner.

Further information about the performance of the different force fields can be obtained from the analysis of the heats of vapourization (see Table 4). The experimental[69] heats of vapourization at 212.77 K and 760 mmHg is 18.67 kJ $mol^{-1}$. The force fields that best reproduce this value are 3S and Kamath, followed closely by 5S. Lower values are predicted by the KL force field (17.33 kJ $mol^{-1}$), while the 5Sd force field predicts a much lower value, around 15.95 kJ $mol^{-1}$). The fact that the 5Sd force field predicts a lower value of heat of vapourization than the rest of the force fields is not surprising, since its dipole moment is almost 50% lower, which decreases significantly the intermolecular interactions. This is in line with what it is observed in other polar molecules, such as water, for which the models usually have dipoles higher than the experimental ones in order to model both gas and liquid properties.

Another property that can help assessing how the force fields perform is the variation of the liquid density with the temperature. We therefore calculated the liquid density that

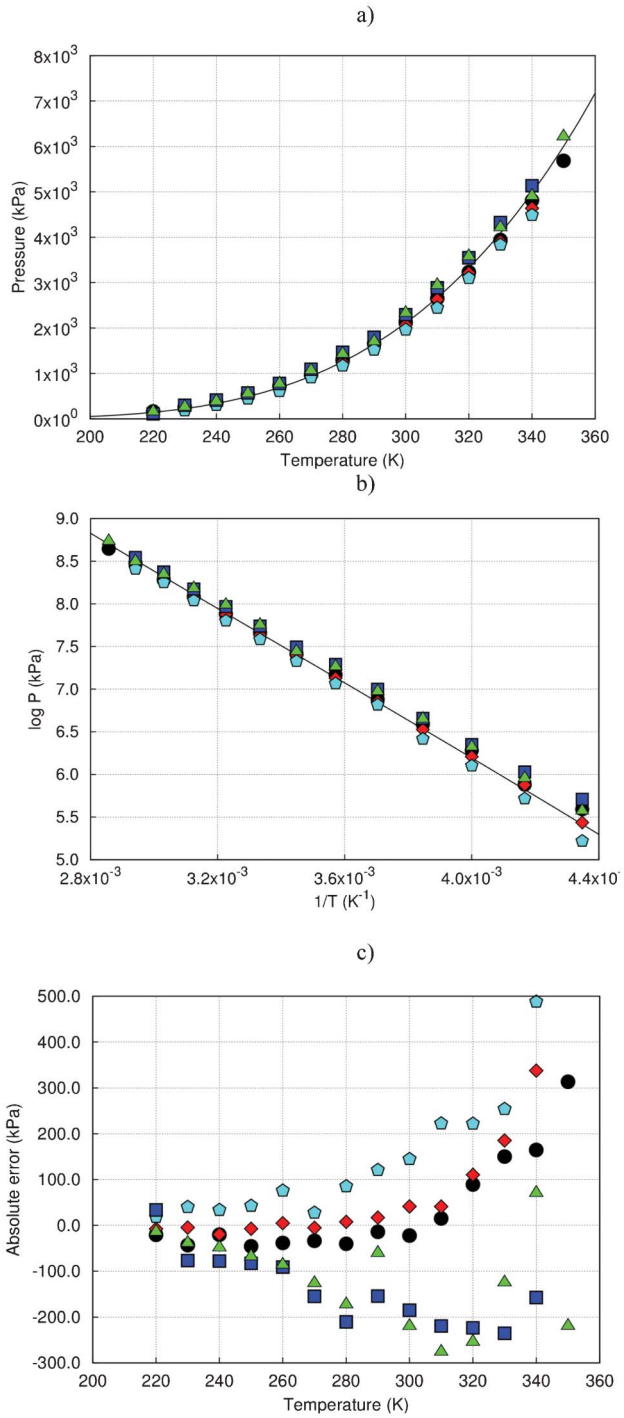


**Fig. 3** a) Experimental[59] vapour pressure curve of $H_2S$ *versus* temperature (line), compared with the simulated curves obtained with the three newly developed force fields, 3S (upwards pointing triangles), 5S (squares) and 5Sd (circles), and the force fields developed by Kristóf and Liszi[23] (diamonds) and Kamath *et al.*[26](pentagons). The same symbols are employed in b) and c). Error bars are not shown, because they would lie within the symbols used to represent the data. b) Logarithm of the vapour pressure *versus* 1/T for the experiment and for the same force fields shown in a). c) Absolute error (respect to the experimental values) of the vapour pressure *versus* temperature, for the same force fields shown in a). The absolute error is defined as the experimental pressure minus the calculated pressure.

**Table 4** Heats of vaporization of $H_2S$, at 212.77 K and 760 mmHg, calculated with the 3S, KL,[23] Kamath,[26] 5S, and 5Sd force fields. The experimental value is also shown[69]

| | Heat of vaporisation (kJ mol$^{-1}$) |
|---|---|
| Experiment | 18.67 |
| 3S | 18.68 |
| KL | 17.33 |
| Kamath | 18.58 |
| 5S | 18.99 |
| 5Sd | 15.93 |

each of them predicts for different temperatures (see Fig. 4), and we find that the 5S and 5Sd force fields are the ones that show the best agreement with the experimental data, followed by the KL and Kamath force fields, and finally the 3S.

We see that none of the force fields outperforms the rest consistently; i. e. the force field that best models some property can also predict another property with the largest error.

In order to investigate the ability of the potentials to model the interaction between $H_2S$ molecules, we can make use of a set of very precise and time-consuming *ab initio* calculations of $H_2S$ dimers carried out by Hellman *et al.*[27] They calculated the dimerisation energy using 16 different dimer structures, the most stable of which is a dimer structure similar to that of most stable water dimer. Its dimerisation energy is −6.6 kJ mol$^{-1}$, which is higher than the value of −2.97 kJ mol$^{-1}$ obtained in previous[70] *ab initio* studies. It is worth noting that the potential energy surface has a very shallow minimum, which suggests that it is quite easy for the $H_2S$ molecules of the dimer to stay far from the minimum, *i.e.* there will not be a significant energy penalty to separate the molecules from the equilibrium distance. If we take into account the fact that the

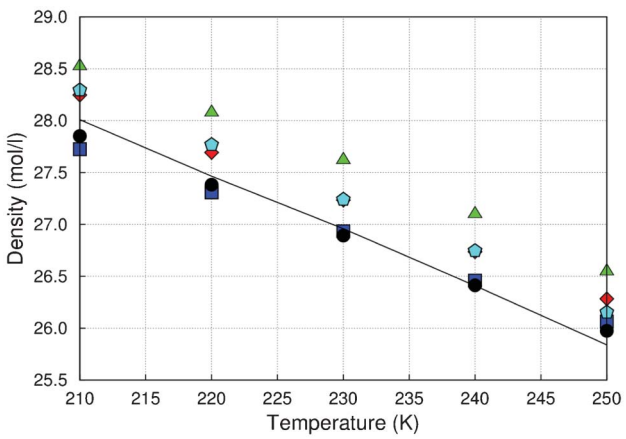


**Fig. 4** Variation of the liquid densities of $H_2S$ (at 0.5 MPa) as a function of temperature. The experimental data[59] (line) are compared with the liquid densities obtained with the three newly developed force fields, 3S (upwards pointing triangles), 5S (squares) and 5Sd (circles), and the force field developed by Kristóf and Liszi[23] (diamonds) and Kamath *et al.*[26](pentagons).

 

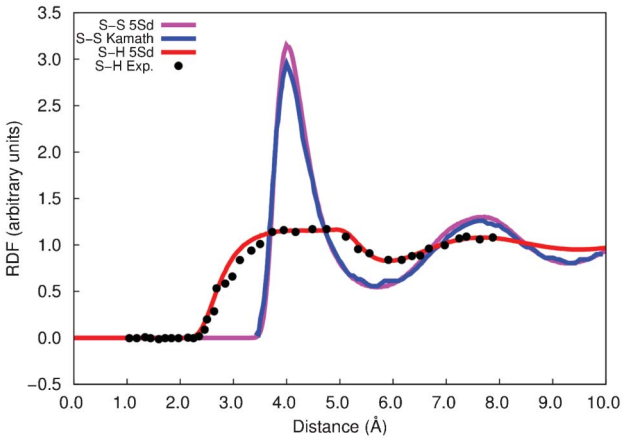


**Fig. 5** S–S and S–H radial distribution functions, at 212.9 K and 1 bar. Experimental values are taken from Andreani *et al.*[71] The values denoted as Kamath are taken from Kamath *et al.*[26]

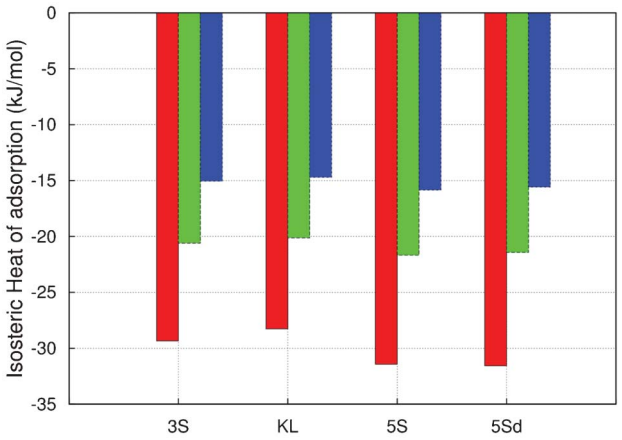


**Fig. 6** Isosteric Heats of adsorption of $H_2S$ adsorbed on three different MOFs, employing the three potential parameters fitted in our study, as well as the KL force field. Red: Cu-BTC. Green: MIL-47. Blue: IRMOF-1.

thermal energy at room temperature is of the order of 2.5 kJ $mol^{-1}$, the electronic structure calculations suggest that $H_2S$ has a very low tendency to form clusters. The S–S distance at which the dimer energy is found is circa 4.1 Å, thus the S–S radial distribution function (RDF) of any simulation of $H_2S$ molecules should present a broad first peak around that distance. And that is indeed what the interatomic potential-based simulations show. In Fig. 5 we report the calculated S–S and S–H RDFs. There are no experimental data to compare the S–S RDF, so in Fig. 5 we can only show the comparison between the S–S RDF (at 212.9 K and 1 bar) calculated by Kamath *et al.*[26] and the one calculated with the 5Sd force field.

Despite being developed with different number of interaction sites, both force fields predict very similar RDFs, which suggests that the VLE curves of $H_2S$ can only be predicted accurately if the S–S interatomic distances vary around 4.1 Å. Regarding S–H distances, since there is no formation of H-bond, there should not be a narrow peak. In fact, this feature can be seen in the experimental S–H RDF (at 212.9 K and 1 bar) shown in Fig. 5, in which there is a broad peak around between radial distances of 3 Å and 5 Å. The Kamath force field was shown[26] to reproduce very well the experimental S–H RDF and that is also the case of the three newly developed force fields. For clarity reasons only the 5Sd S–H RDF is shown in Fig. 5, although those of 3S and 5S are very close, they would lie within the symbols employed to represent them. There is a very good agreement between simulated (with both the Kamath and 5Sd force fields) and experimental S–H RDFs, which suggests that the underlying physics of the intermolecular interactions are described correctly by the force fields employed.

### B) Modelling of the adsorption properties of $H_2S$ on three materials

The potential parameters which we have developed allow us to calculate the adsorption energies of $H_2S$ on any porous materials for which we already know the Lennard–Jones parameters that best model them. To calculate the potential parameters for the guest-host interactions we make use of the Lorentz–Berthelot mixing rules. To investigate the influence of the $H_2S$ potential parameters on the adsorption properties we studied the adsorption of $H_2S$ on Cu-BTC, MIL-47, and IRMOF-1. Fig. 6 shows the isosteric Heats of adsorption obtained with the four sets of potential parameters.

For all materials, the 4S potential predicts slightly lower Heats of adsorption than the 3S potential, while the 5S potential predicts consistently higher values of Heats of adsorption. The material for which the Heat of adsorption is higher is Cu-BTC, since the molecule confines better in the tetrahedral-shaped pockets of this structure than in the wider pores of MIL-47 and IRMOF-1. The three potentials predict Heats of adsorption in Cu-BTC ranging from $-28$ kJ $mol^{-1}$ to $-32$ kJ $mol^{-1}$. In the case of MIL-47 the values range between $-20$ kJ $mol^{-1}$ and $-22$ kJ $mol^{-1}$. And the lowest Heats of adsorption correspond to IRMOF-1, for which the predicted values vary from $-14$ kJ $mol^{-1}$ to $-16$ kJ $mol^{-1}$. This behaviour can be readily understood by considering the respective values of the interaction parameters shown in Table 2. The values of the $\sigma$ parameters are almost the same in the four force fields, but the values of the $\varepsilon$ do vary significantly, following the order KL $<$ 3S $<$ 5S $<$ 5Sd. And this is indeed the ordering that we observe for the values of the Heats of adsorption. There is only a slight change in this trend for 5S and 5Sd, since the former has a smaller value of the $\varepsilon$ parameter but it predicts a larger value of the Heat of adsorption than 5Sd. This difference of the $\varepsilon$ parameter is compensated by the difference of molecular dipole, which is 50% larger for 5S than for 5Sd.

There is no experimental data available for comparison, but, since the three potentials predict similar values of Heats of adsorption, it would not be possible to rule out the capability of any of them to model the system correctly, based only on this property. Due to this lack of experimental data, we carried out electronic structure calculations, which provide independent information with which we could compare the Heats of adsorption of $H_2S$. Watanabe and Sholl carried out a periodic

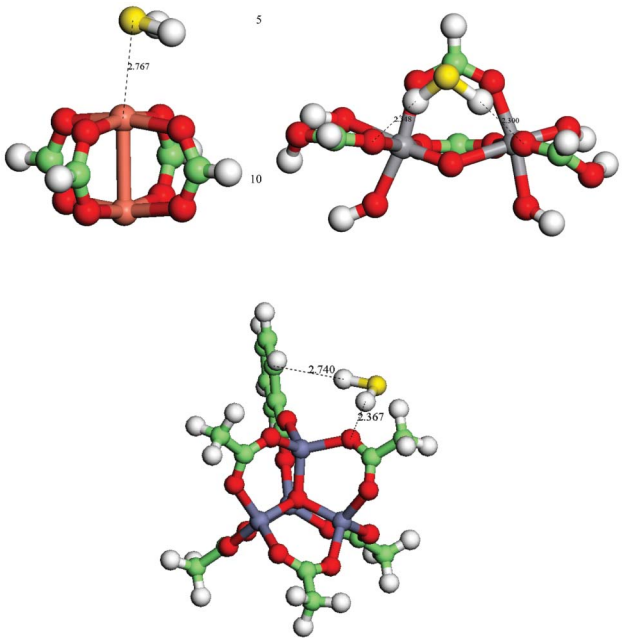


**Fig. 7** Minimum energy configurations of $H_2S$ adsorbed on three clusters models of (from left to right) Cu-BTC, MIL-47, and IRMOF-1. The energy minimizations were carried out with DFT calculations, employing the M06-2X exchange–correlation functional. The cluster models of the surfaces are kept fixed during the minimizations.

DFT study[31] (using the PW91 exchange–correlation functional[72] with an energy cutoff of 500 eV) of $H_2O$ and $H_2S$ adsorption on Cu-BTC. They found that the adsorption energy of a $H_2O$ molecule is $-41.0$ kJ mol$^{-1}$, while that of a $H_2S$ molecule is $-31.2$ kJ mol$^{-1}$. We have carried out DFT calculations on the cluster models of the systems shown in Fig. 7, employing the M06-2X functional mentioned in the computational details. The BSSE-corrected energies of adsorption of $H_2S$ and $H_2O$ on the three materials are shown in Table 5. We have obtained values of adsorption energies for $H_2O$ and $H_2S$ of $-46.7$ kJ mol$^{-1}$ and $-43.4$ kJ mol$^{-1}$ respectively, which are higher than the energies obtained by Watanabe and Sholl.[31] This is not surprising, since the PW91 functional was not developed to include accurately the non covalent interactions that are important in this system.

Grajciar *et al.*[73] employed very accurate CCSD(T)/CBS calculations (on the same cluster model we have studied) and obtained an energy of adsorption of $-52$ kJ mol$^{-1}$ for $H_2O$ molecules on Cu-BTC. This value of adsorption energy is close to that predicted by our calculations, $-46.7$ kJ mol$^{-1}$, suggesting that the M06-2X calculations are accurate enough to provide reliable predictions of adsorption energies, at a fraction of the cost of CCSD(T)/CBS calculations. The adsorption energy predicted by the DFT calculations for the $H_2S$ molecule is $-43.4$ kJ mol$^{-1}$, which is higher than the values for Heats of adsorption obtained from the Monte Carlo simulations (between $-28$ kJ mol$^{-1}$ and $-32$ kJ mol$^{-1}$). This suggest that the force fields 5S and 5Sd give the best description of the adsorption energy in Cu-BTC, followed by 3S, with KL giving the lower adsorption energy.

**Table 5** Energies of adsorption of $H_2S$ and $H_2O$ on the three cluster models of Cu-BTC, MIL-47 and IRMOF-1 shown in Fig. 7. The energies are BSSE-corrected and they are calculated with DFT, using the M06-2X exchange–correlation functional[54]

| | $H_2S$ Adsorption energy (kJ mol$^{-1}$) | $H_2O$ Adsorption energy (kJ mol$^{-1}$) |
|---|---|---|
| Cu-BTC | $-43.4$ | $-46.7$ |
| MIL-47 | $-33.9$ | $-41.0$ |
| IRMOF-1 | $-16.7$ | $-22.5$ |

For IRMOF-1 all the force fields predict similar values of isosteric Heat of adsorption, around $-15$ kJ mol$^{-1}$, which is very close to the adsorption energy of $-16.7$ kJ mol$^{-1}$ obtained with DFT calculations. Something similar occurs in the case of the adsorption in MIL-47, for which there are experimental data to compare with. Hamon *et al.*[15] found experimental values of adsorption energy for MIL-47 from $-27$ kJ mol$^{-1}$ to $-29$ kJ mol$^{-1}$. But all the force fields studied predict this energy to be between $-20$ kJ mol$^{-1}$ (for KL) and $-22$ kJ mol$^{-1}$ (for 5S). Our DFT calculations predict an adsorption energy of $-33.9$ kJ mol$^{-1}$, which is slightly closer to the experimental values. It is puzzling to find that all the force fields predict similar values of adsorption energy for each of the three materials studied, independently of how their parameters where fitted. At first sight it would be easy to assign the origin of this fact to the only common value in all the force fields, which is the $\sigma$ parameter (it has a value that only varies from 3.70 Å to 3.75 Å among all the force fields). But this assumption does not hold true. We performed an additional study on the variation of the adsorption energy of $H_2S$ in IRMOF-1 changing independently the $\sigma$ and $\varepsilon$ parameters by 8%. Our results show that both parameters are equally important, causing a change of the adsorption energy of circa 5% and 8% for the variation of the $\varepsilon$ and $\sigma$ parameters respectively.

We could therefore conclude that out of the three potential parameters we have developed for $H_2S$, 3S, 5S, and 5Sd (which predict higher adsorption energies) are the ones that predict values of the adsorption energies in closer agreement with the DFT data, although the energy differences are so small that it is not possible to rule out the validity of any of the force fields.

As to the distance at which the $H_2S$ molecule is predicted to stay from the framework, the DFT calculations do have a minimum energy configuration when the S atom of the $H_2S$ molecule is at 2.6 Å from the Cu atom of the Cu-BTC framework. Since the DFT calculations do not include neither thermal effects nor the effects of $H_2S$-$H_2S$ interactions, the S–Cu distance predicted with them is expected to be shorter than that predicted with Monte Carlo simulations, which is around 3.1 Å, as can be seen in Fig. 8a, where for clarity reasons only the results for KL and 5Sd are shown, although the other force fields predict similar RDFs.

It was previously observed[15] that the presence of the MIL-47 framework influences the interatomic interactions, so that the S–H RDF of liquid $H_2S$ is very different to that obtained when $H_2S$ is adsorbed. Fig. 8b shows that is also observed when the

 

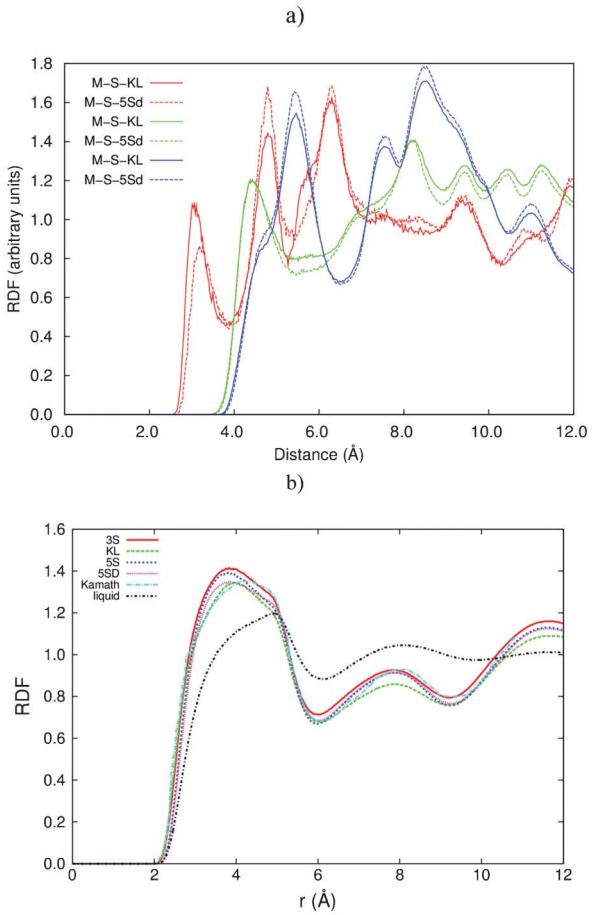


**Fig. 8** a) Calculated M-S radial distribution functions at 303 K, where M is the metal atoms of the framework: Cu in Cu-BTC (red), Zn in IRMOF-1 (green), and V in MIL-47 (blue). b) H($H_2S$)-S($H_2S$) RDFs of H2S adsorbed in MIL-47, calculated with the 3S,5S, 5Sd, KL, and Kamath force fields, at 1 bar and 303 K. The results for the Kamath force field are taken from Hamon *et al.*[15] The RDF in the liquid phase is also shown here for comparison.

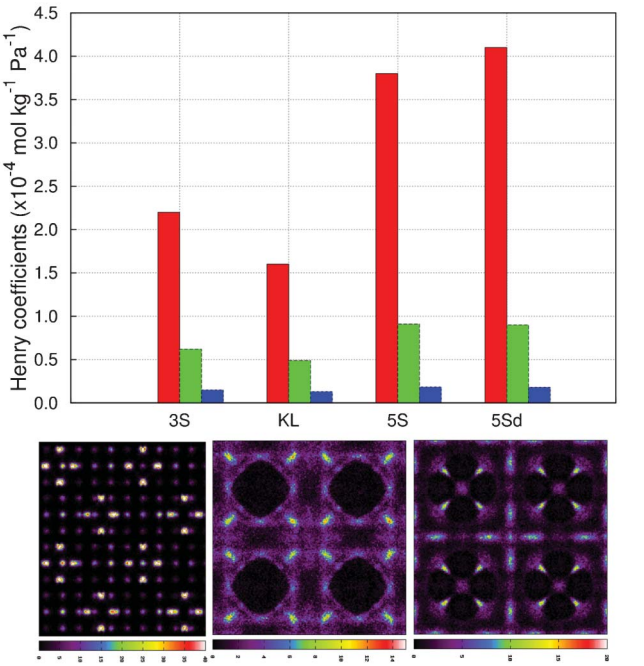


**Fig. 9** Top panel: Henry coefficients of $H_2S$ for three different materials at 298 K, employing the KL, 3S, 5S and 5Sd potential parameters. Red: Cu-BTC. Green: MIL-47. Blue: IRMOF-1. Bottom panel: Average occupation profiles of the $H_2S$ centre of mass (at 100 kPa) on Cu-BTC, IRMOF-1 and MIL-47, using the 5Sd force field.

new force fields are employed. The confinement makes the first S–H peak to grow and displace towards a shorter distance.

Another factor that provides valuable information regarding the adsorption behavior is the Henry coefficient, which is defined as $k_H = C/P$, where $P$ is the pressure of the system and $C$ is the $H_2S$ loading. The values of the Henry coefficients obtained from our simulations are shown in the top panel of Fig. 9. As in the case of the Heats of adsorption, the 5S and 5Sd potentials predict higher values of the Henry coefficients than the other force fields, for the same reason that mentioned when discussing the Heats of adsorption. As to the dependence of the Henry coefficients with the type of material, it can be explained by analyzing the different sites in which the $H_2S$ molecules are adsorbed for each material. Cu-BTC adsorbs $H_2S$ molecules preferentially confining them inside small cages (see the bottom panel of Fig. 9), which increases the value of $k_H$. MIL-47 has some kinks in the structure, where $H_2S$ molecules are adsorbed, while IRMOF-1 has large cages where the $H_2S$ molecules are adsorbed, thus inducing lower values of $k_H$ than the other two structures.

There is only one experimental value of $k_H$ for any of the three materials studied, which was obtained by Hamon *et al.*[15] for MIL-47. They obtained two values of $k_H$, one corresponding to a linear region at pressures below 25 kPa ($0.47 \times 10^{-4}$ mol kg$^{-1}$ Pa$^{-1}$), and another one corresponding to a linear region at pressures between 25 and 30 kPa ($0.81 \times 10^{-4}$ mol kg$^{-1}$ Pa$^{-1}$). The KL force field predicts a value of $k_H$ ($0.49 \times 10^{-4}$ mol kg$^{-1}$ Pa$^{-1}$) which is very close to the experimental one at low pressures. The value predicted by the 3S force fields is slightly higher ($0.60 \times 10^{-4}$ mol kg$^{-1}$ Pa$^{-1}$), while those predicted by the two five-sites force fields are much higher (around $0.90 \times 10^{-4}$ mol kg$^{-1}$ Pa$^{-1}$).

The analysis of the Henry coefficients seems to suggest that the KL force field could provide a better description of the adsorption of $H_2S$ in MIL-47. But given the usually large errors involved both in the experimental measurements of the Henry coefficients and in their theoretical calculation, we could not conclude that the KL is definitely better suited than any of the others to model $H_2S$ adsorbed in MIL-47.

The adsorption isotherms of $H_2S$ on Cu-BTC, IRMOF-1, and MIL-47, calculated with the three potentials developed in this study, are shown in Fig. 10. The most remarkable feature observed in the adsorption isotherms is that the 5S potential predicts similar values of adsorption for low and high pressures than the rest of the potentials, but in the transition regions it predicts higher adsorption for the three materials than the other potentials. This implies that the adsorbed molecules pack in a slightly different way depending on the potential used. Another remarkable feature is the fact that the

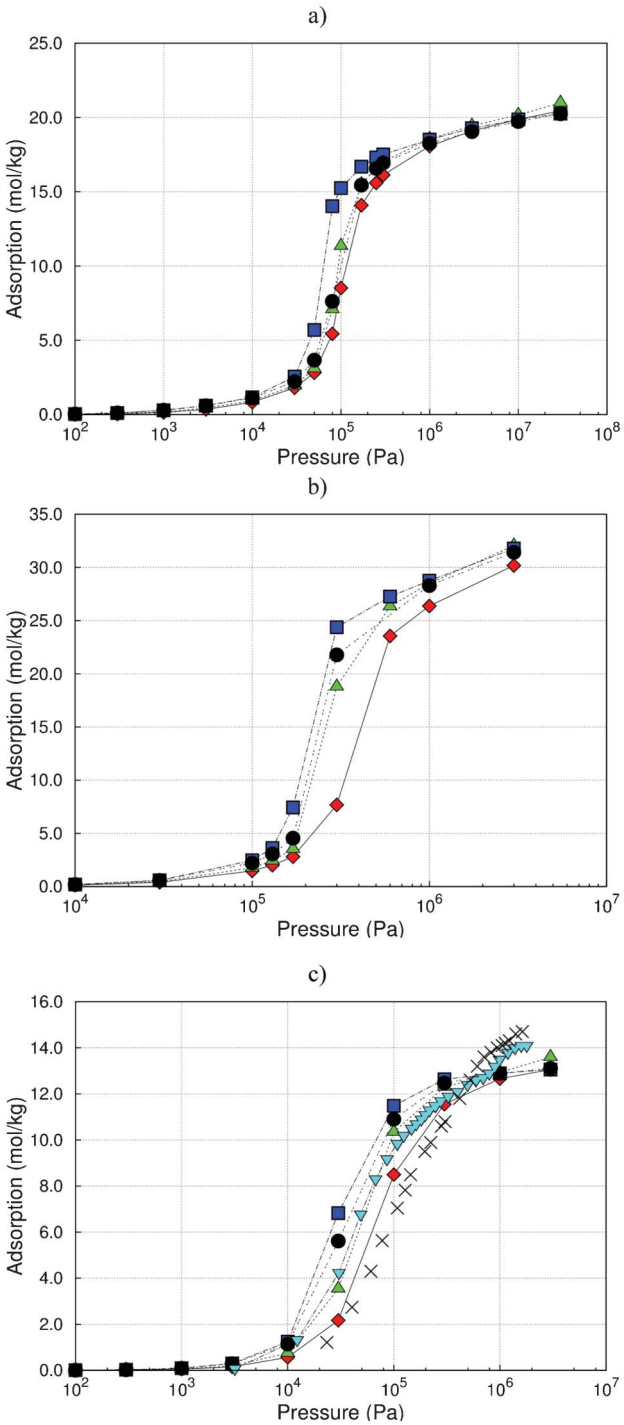


**Fig. 10** Adsorption isotherms (at 300 K) of $H_2S$ adsorbed in Cu-BTC (a), IRMOF-1 (b) and MIL-47 (c), using the three potentials developed in this study, 3S (upwards pointing triangles), 5S (squares), 5Sd (circles), as well as the force field developed by Kristóf and Liszi[23] (diamonds). Previous experimental[15] data (crosses) of adsorption on MIL-47 (at 303 K) are included for comparison. For this material we also show (downwards pointing triangles) the adsorption isotherm calculated by Hamon *et al.*[15] employing with the Kamath force field.

KL force field consistently predict lower adsorption values than the rest of the force fields. There are not enough experimental values to test which of the models provides a better agreement with experiment. The only experimental isotherm that of MIL-47, which is shown in Fig. 10c. The best agreement is found for the KL force field, followed closely by the 3S and Kamath force fields. Although, due to the large variation of the experimental adsorption isotherms, is it necessary to compare with more than one isotherm, once a reasonable consensus is found as to what the adsorption isotherm is.[50,74–77]

With the results obtained so far we can shed some light into the interpretations of the experimental data regarding $H_2S$ adsorption in Cu-BTC. In an experimental study Petit *et al.*[9] found that Cu-BTC is degraded upon adsorption of $H_2S$. They proposed a mechanism for the Cu-BTC crystal degradation, which is based on the assumption that $H_2S$ does bind strongly to the Cu atoms and is able to replace water molecules present at those sites. Nevertheless, our simulations (both classical and Quantum-based simulations) do not agree with that view, *i.e.* water is predicted to bind more strongly to Cu-BTC than $H_2S$. This is observed for every force field studied and confirmed not only by our hybrid DFT calculations of the cluster model of the system, but also by a previous study,[31] which employs a different kind of calculation, namely periodical plane waves DFT. We carried out a study of the dipole moment that $H_2S$ molecules would need to have in order to replace the water molecules. We found that, for a temperature of 300 K and a pressure of 10 kPa, as the dipole increases from 0.95 D to 1.95 D there is a small, gradual increase of adsorption, from 1.2 mol $kg^{-1}$ to 2 mol $kg^{-1}$ (see ESI†). But when the dipole has the extremely high value of 2.1 D the adsorption abruptly increases to values higher than 15 mol $kg^{-1}$. But this sudden increase of adsorption is not due to a stronger interaction with the Cu atoms, but to stronger intermolecular interactions, i. e. the higher dipole causes the $H_2S$ molecules to nucleate and form clusters, away from the Cu atoms (see ESI†).

In an attempt to test whether the mechanism proposed by Petit *et al.* is confirmed by DFT simulation, we tried to calculate the difference in Gibbs Free energy between the $H_2S$ molecule adsorbed on the cluster shown in Fig. 7a and different reaction states, such as 1) the S atom bonded to the Cu atom with the two H atoms desorbed, forming a $H_2$ molecule; 2) the S atom bonded to the Cu atom and to one H atom, with the remaining H atom either desorbed or bonded to an O atom that has broken its bond to the Cu atom. Unfortunately, all these structures are so unstable that in none of them the SCF cycles could achieve convergence.

In order to get a further insight into the interaction between the Cu-BTC structure and $H_2S$ and $H_2O$ molecules we carried out *ab initio* molecular dynamics of the molecules adsorbed on the model cluster shown in Fig. 7, employing the Atom-Centered Density Matrix Propagation molecular dynamics method,[78,79] as implemented in Gaussian 09. In this method the nuclear degrees of freedom are treated with quantum mechanics, while the electronic degrees of freedom are propagated adiabatically, employing an extended Lagrangian approach. The level of theory used is HF/LanL2MB.[80] The calculations were 3 ps long, with a time step of 0.1 fs, and the temperature was 300 K. The simulations show that here is a large difference of adsorption between the two molecules,

 

since the $H_2O$ molecule stays close to the cluster, at an average distance from the Cu atom of circa 2.7 Å, while the $H_2S$ molecule is desorbed and leaves the cluster, reaching distances of circa 5.3 Å. Snapshots of these simulations are shown in the ESI.† This new piece of information is in line with the other theoretical results, so it is then clear that all types of simulations agree on the prediction that the interaction between $H_2S$ and Cu-BTC is much weaker than that of $H_2O$. There seems to be an apparent discrepancy between experimental and theoretical results. But we would like to note that there is not really a contradiction, since it would be possible that another mechanism not yet presented could explain the reasons why $H_2S$ degrades the crystalline structure, even in the presence of water molecules, which interact more strongly with the Cu atoms. This is an interesting problem that deserves further studies.

## IV. Conclusions

We have developed three new force fields that model the liquid and gas phases of $H_2S$ correctly. All previous force fields include long-range corrections to the Lennard–Jones energy, so in order to check whether other force fields with different fitting procedures to the previously published ones would yield different description of the adsorption properties in microporous materials (particularly in Metal–Organic Frameworks), we applied a cut and shift of the Lennard–Jones energy. Moreover we employed various values of the molecular dipole moment and different number of interaction sites. Two of the force fields have a molecular dipole (1.43 D) higher than the one obtained experimentally (0.974 D), and one has the experimental dipole. The fitting of the parameters was carried out employing Gibbs ensemble Monte Carlo simulations, with which we obtained three sets of interatomic potentials that model the experimental properties of liquid and gaseous $H_2S$. Comparing the results of the interatomic potential-based adsorption simulations on Cu-BTC, MIL-47, and IRMOF-1 with those obtained with DFT calculations, we have found that the newly developed potentials do provide reliable results and could therefore be employed in further studies of $H_2S$ adsorption. But the improvement of the description of the electrostatic potential around the molecule achieved by the models with a larger number of point charges (5S and 5Sd models) does not necessarily imply that the interaction between the $H_2S$ molecules and the framework is better modelled with those force fields.

Our study also sheds some light into the mechanisms by which Cu-BTC degrades when $H_2S$ is adsorbed. Experimental studies suggest that the interaction between $H_2S$ and the Cu atom in Cu-BTC is strong, with $H_2S$ molecules being able to displace $H_2O$ molecules. But the results of the simulations, performed both with the new force fields and with the previous ones, suggest otherwise, $H_2O$ does interact with the Cu atoms more strongly than $H_2S$, which stays in the cages of the framework. DFT calculations predict similar results compared with classical simulations. Our simulation study therefore suggests that there must be something missing in the mechanisms proposed so far to explain the degradation observed in Cu-BTC upon adsorption of $H_2S$.

## Acknowledgements

This work is supported by the Spanish MICINN (CTQ2010-16077) and by the European Research Council through an ERC Starting Grant ERC_279520 (S. Calero). JJGS thanks MEC (CTQ2007-63229) for his predoctoral fellowship. AMC thanks MEC for her predoctoral fellowship.

## References

1 J. W. v. Groenestijn and N. J. R. Kraakman, *Chem. Eng. J.*, 2005, **113**, 85–91.
2 M. P. Cal, B. W. Strickler, A. A. Lizzio and S. K. Gangwal, *Carbon*, 2000, **38**, 1767–1774.
3 K. Polychronopoulou, J. L. G. Fierro and A. M. Efstathiou, *Appl. Catal., B*, 2005, **57**, 125–137.
4 Y. Xiao, S. Wang, D. Wu and Q. Yuan, *J. Hazard. Mater.*, 2008, **153**, 1193–1200.
5 K. Kim and N. Park, *J. Ind. Eng. Chem.*, 2010, **16**, 967–972.
6 H. R. Godini and D. Mowla, *Chem. Eng. Res. Des.*, 2008, **86**, 401–409.
7 S. A. M. Marzouk, M. H. Al-Marzouqi, N. Abdullatif and Z. M. Ismail, *J. Membr. Sci.*, 2010, **360**, 436–441.
8 I. Novochinskii, C. S. Song, X. L. Ma, X. S. Liu, L. Shore, J. Lampert and R. J. Farrauto, *Energy Fuels*, 2004, **18**, 576–583.
9 C. Petit, B. Mendoza and T. J. Bandosz, *ChemPhysChem*, 2010, **11**, 3678–3684.
10 O. K. Farha, A. Ö. Yazaydin, I. Eryazici, C. D. Malliakas, B. G. Hauser, M. G. Kanatzidis, S. T. Nguyen, R. Q. Snurr and J. T. Hupp, *Nat. Chem.*, 2010, **2**, 944–948.
11 H. Li, M. Eddaoudi, M. O'Keeffe and O. M. Yaghi, *Nature*, 1999, **402**, 276–279.
12 H. C. Zhou, J. R. Long and O. M. Yaghi, *Chem. Rev.*, 2012, **112**, 673–674.
13 T. K. Trung, P. Trens, N. Tanchoux, S. Bourrelly, P. L. Llewellyn, S. Loera-Serna, C. Serre, T. Loiseau, F. o. Fajula and G. r. FeÌrey, *J. Am. Chem. Soc.*, 2008, **130**, 16926–16932.
14 P. Horcajada, C. Serre, G. Maurin, N. A. Ramsahye, F. Balas, M. Vallet-Regí, M. Sebban, F. Taulelle and G. Férey, *J. Am. Chem. Soc.*, 2008, **130**, 6774–6780.
15 L. Hamon, H. Leclerc, A. Ghoufi, L. Oliviero, A. Travert, J.-C. Lavalley, T. Devic, C. Serre, G. Férey, G. De Weireld, A. Vimont and G. Maurin, *J. Phys. Chem. C*, 2011, **115**, 2047–2056.
16 J. L. C. Rowsell and O. M. Yaghi, *Microporous Mesoporous Mater.*, 2004, **73**, 3–14.
17 S. S. Y. Chui, S. M. F. Lo, J. P. H. Charmant, A. G. Orpen and I. D. Williams, *Science*, 1999, **283**, 1148–1150.
18 J. R. Li, R. J. Kuppler and H. C. Zhou, *Chem. Soc. Rev.*, 2009, **38**, 1477–1504.
19 A. U. Czaja, N. Trukhan and U. Muller, *Chem. Soc. Rev.*, 2009, **38**, 1284–1293.
20 K. Barthelet, J. Marrot, D. Riou and G. Ferey, *Angew. Chem., Int. Ed.*, 2002, **41**, 281.

21 W. L. Jorgensen, J. D. Madura and C. J. Swenson, *J. Am. Chem. Soc.*, 1984, **106**, 6638–6646.
22 T. R. Forester, I. R. McDonald and M. L. Klein, *Chem. Phys.*, 1989, **129**, 225–234.
23 T. Kristóf and J. Liszi, *J. Phys. Chem. B*, 1997, **101**, 5480–5483.
24 J. Delhommelle, P. Millié and A. H. Fuchs, *Mol. Phys.*, 2000, **98**, 1895–1905.
25 W. Lin, Q. Yang and C. Zhong, *Fluid Phase Equilib.*, 2004, **220**, 1–6.
26 G. Kamath, N. Lubna and J. J. Potoff, *J. Chem. Phys.*, 2005, **123**, 124505.
27 R. Hellmann, E. Bich, E. Vogel and V. Vesovic, *Phys. Chem. Chem. Phys.*, 2011, **13**, 13749–13758.
28 W. L. Jorgensen, *J. Phys. Chem.*, 1986, **90**, 6379–6388.
29 T. J. Bandosz and C. Petit, *Dalton Trans.*, 2012, **41**, 4027–4035.
30 T. Bandosz, *Activated Carbon Surfaces in Environmental Remediation*, Academic Press, Oxford, UK, 2006.
31 T. Watanabe and D. S. Sholl, *J. Chem. Phys.*, 2010, **133**, 094509.
32 J. M. Castillo, T. J. H. Vlugt and S. Calero, *J. Phys. Chem. C*, 2008, **112**, 15934–15939.
33 J. M. Sorenson, G. Hura, R. M. Glaeser and T. Head-Gordon, *J. Chem. Phys.*, 2000, **113**, 9149.
34 C. Andreani, V. Merlo, M. A. Ricci, G. Ruocco and A. K. Soper, *Europhys. Lett.*, 1989, **8**, 441–446.
35 R. D. Goodwin, Hydrogen Sulfide Provisional Thermophysical Properties from 188 to 700K at Pressures to 75 MPa, NBSIR 83-1694, Nat. Bureau Stds., 1983.
36 T. Kristóf and J. Liszi, *Mol. Phys.*, 1997, **90**, 1031–1034.
37 G. Galliero, C. Nieto-Draghi, C. Boned, J. B. Avalos, A. D. Mackie, A. Baylaucq and F. Montel, *Ind. Eng. Chem. Res.*, 2007, **46**, 5238–5244.
38 M. Eddaoudi, J. Kim, N. Rosi, D. Vodak, J. Wachter, M. O'Keeffe and O. M. Yaghi, *Science*, 2002, **295**, 469–472.
39 S. L. Mayo, B. D. Olafson and W. A. Goddard, *J. Phys. Chem.*, 1990, **94**, 8897–8909.
40 A. K. Rappe, C. J. Casewit, K. S. Colwell, W. A. Goddard and W. M. Skiff, *J. Am. Chem. Soc.*, 1992, **114**, 10024–10035.
41 H. Frost and R. Q. Snurr, *J. Phys. Chem. C*, 2007, **111**, 18794–18803.
42 D. Dubbeldam, K. S. Walton, D. E. Ellis and R. Q. Snurr, *Angew. Chem., Int. Ed.*, 2007, **46**, 4496–4499.
43 R. Bueno-Perez, E. Garcia-Perez, J. Jose Gutierrez-Sevillano, P. J. Merkling and S. Calero, *Adsorpt. Sci. Technol.*, 2010, **28**, 823–835.
44 J. Getzschmann, I. Senkovska, D. Wallacher, M. Tovar, D. Fairen-Jimenez, T. Duren, J. M. van Baten, R. Krishna and S. Kaskel, *Microporous Mesoporous Mater.*, 2010, **136**, 50–58.
45 A. Martin-Calvo, E. Garcia-Perez, J. M. Castillo and S. Calero, *Phys. Chem. Chem. Phys.*, 2008, **10**, 7085–7091.
46 J. M. Castillo, T. J. H. Vlugt and S. Calero, *J. Phys.Chem. C*, 2009, **113**, 20869–20874.
47 D. Dubbeldam, H. Frost, K. S. Walton and R. Q. Snurr, *Fluid Phase Equilib.*, 2007, **261**, 152–161.
48 D. Frenkel and B. Smit, *Understanding Molecular Simulation From Algorithms to Applications*, second edition edn, Academic Press, San Diego. C. A., 2002.
49 S. Calero, A. Martin-Calvo, S. Hamad and E. Garcia-Perez, *Chem. Commun.*, 2011, **47**, 508–510.
50 A. Garcia-Sanchez, C. O. Ania, J. B. Parra, D. Dubbeldam, T. J. H. Vlugt, R. Krishna and S. Calero, *J. Phys. Chem. C*, 2009, **113**, 8814–8820.
51 T. J. H. Vlugt, E. Garcia-Perez, D. Dubbeldam, S. Ban and S. Calero, *J. Chem. Theory Comput.*, 2008, **4**, 1107–1118.
52 A. Martín-Calvo, E. García-Pérez, J. M. Castillo and S. Calero, *Phys. Chem. Chem. Phys.*, 2008, **10**, 7085–7091.
53 M. J. Frisch, G. W. Trucks, H. B. Schlegel, G. E. Scuseria, M. A. Robb, J. R. Cheeseman, G. Scalmani, V. Barone, B. Mennucci, G. A. Petersson, H. Nakatsuji, M. Caricato, X. Li, H. P. Hratchian, A. F. Izmaylov, J. Bloino, G. Zheng, J. L. Sonnenberg, M. Hada, M. Ehara, K. Toyota, R. Fukuda, J. Hasegawa, M. Ishida, T. Nakajima, Y. Honda, O. Kitao, H. Nakai, T. Vreven, J. J. A. Montgomery, J. E. Peralta, F. Ogliaro, M. Bearpark, J. J. Heyd, E. Brothers, K. N. Kudin, V. N. Staroverov, R. Kobayashi, J. Normand, K. Raghavachari, A. Rendell, J. C. Burant, S. S. Iyengar, J. Tomasi, M. Cossi, N. Rega, J. M. Millam, M. Klene, J. E. Knox, J. B. Cross, V. Bakken, C. Adamo, J. Jaramillo, R. Gomperts, R. E. Stratmann, O. Yazyev, A. J. Austin, R. Cammi, C. Pomelli, J. W. Ochterski, R. L. Martin, K. Morokuma, V. G. Zakrzewski, G. A. Voth, P. Salvador, J. J. Dannenberg, S. Dapprich, A. D. Daniels, Ö. Farkas, J. B. Foresman, J. V. Ortiz, J. Cioslowski and D. J. Fox, Gaussian, Inc., Wallingford CT, 2009, pp. Gaussian 09, Revision A.01; M. J. Frisch, G. W. Trucks, H. B. Schlegel, G. E. Scuseria, M. A. Robb, J. R. Cheeseman, G. Scalmani, V. Barone, B. Mennucci, G. A. Petersson, H. Nakatsuji, M. Caricato, X. Li, H. P. Hratchian, A. F. Izmaylov, J. Bloino, G. Zheng, J. L. Sonnenberg, M. Hada, M. Ehara, K. Toyota, R. Fukuda, J. Hasegawa, M. Ishida, T. Nakajima, Y. Honda, O. Kitao, H. Nakai, T. Vreven, J. J. A. Montgomery, J. E. Peralta, F. Ogliaro, M. Bearpark, J. J. Heyd, E. Brothers, K. N. Kudin, V. N. Staroverov, R. Kobayashi, J. Normand, K. Raghavachari, A. Rendell, J. C. Burant, S. S. Iyengar, J. Tomasi, M. Cossi, N. Rega, J. M. Millam, M. Klene, J. E. Knox, J. B. Cross, V. Bakken, C. Adamo, J. Jaramillo, R. Gomperts, R. E. Stratmann, O. Yazyev, A. J. Austin, R. Cammi, C. Pomelli, J. W. Ochterski, R. L. Martin, K. Morokuma, V. G. Zakrzewski, G. A. Voth, P. Salvador, J. J. Dannenberg, S. Dapprich, A. D. Daniels, Ö. Farkas, J. B. Foresman, J. V. Ortiz, J. Cioslowski and D. J. Fox, Gaussian, Inc., Wallingford CT, 2009, pp. Gaussian 09, Revision A.01.
54 Y. Zhao and D. G. Truhlar, *Theor. Chem. Acc.*, 2008, **120**, 215–241.
55 D. Tzeli, I. D. Petsalakis, G. Theodorakopoulos, D. Ajami and J. Rebek, *Int. J. Quantum Chem.*, 2013, **113**, 734–739.
56 D. Tzeli, I. D. Petsalakis and G. Theodorakopoulos, *J. Phys. Chem. A*, 2011, **115**, 11749–11760.
57 P. Fuentealba, H. Preuss, H. Stoll and L. v. Szentpaly, *Chem. Phys. Lett.*, 1982, **89**, 418–422.
58 S. Simon, M. Duran and J. J. Dannenberg, *J. Chem. Phys.*, 1996, **105**, 11024–11031.
59 http://webbook.nist.gov/chemistry/, *National Institute of Standards and Technology*.
60 C. Huiszoon and A. Dymanus, *Physica*, 1965, **31**, 1049–1052.

 

61 R. C. Weast, *Handbook of Chemistry and Physics*, 67 edn, Boca Raton: CRC Press, 1986.
62 M. P. Allen and D. J. Tildesley, *Computer Simulation of Liquids*, Oxford University Press, USA, 1989.
63 M. D. Macedonia and E. J. Maginn, *Mol. Phys.*, 1999, **96**, 1375–1390.
64 F. Siperstein, A. L. Myers and O. Talu, *Mol. Phys.*, 2002, **100**, 2025–2030.
65 P. W. Atkins, *Physical Chemistry*, Oxford Higher Education, New York, 1990.
66 M. G. Martin and J. I. Siepmann, *J. Phys. Chem. B*, 1998, **102**, 2569–2577.
67 J. S. Rowlinson and F. L. Swinton, *Liquids and Liquid Mixtures*, 3rd edn, Butterworth, London, 1982.
68 J. S. Rowlinson and B. Widom, *Molecular Theory of Capillarity*, Oxford University Press, New York, 1989.
69 W. F. Giauque and R. W. Blue, *J. Am. Chem. Soc.*, 1936, **58**, 831.
70 J. R. Sabin, *J. Am. Chem. Soc.*, 1971, **93**, 3613–3620.
71 C. Andreani, V. Merlo, M. A. Ricci and A. K. Soper, *Mol. Phys.*, 1991, **73**, 407.
72 J. P. Perdew and Y. Wang, *Phys. Rev. B: Condens. Matter*, 1992, **45**, 13244.
73 L. Grajciar, O. Bludský and P. Nachtigall, *J. Phys. Chem. Lett.*, 2010, **1**, 3354–3359.
74 P. Chowdhury, C. Bikkina, D. Meister, F. Dreisbach and S. Gumma, *Microporous Mesoporous Mater.*, 2009, **117**, 406.
75 A. Figini-Albisetti, L. F. Velasco, J. B. Parra and C. O. Ania, *Appl. Surf. Sci.*, 2010, **256**, 5182.
76 D. Dubbeldam, S. Calero, T. J. H. Vlugt, R. Krishna, T. L. M. Maesen and B. Smit, *J. Phys. Chem. B*, 2004, **108**, 12301.
77 S. Calero, D. Dubbeldam, R. Krishna, B. Smit, T. J. H. Vlugt, J. F. M. Denayer, J. A. Martens and T. L. M. Maesen, *J. Am. Chem. Soc.*, 2004, **126**, 11377–11386.
78 H. B. Schlegel, S. S. Iyengar, X. Li, J. M. Millam, G. A. Voth, G. E. Scuseria and M. J. Frisch, *J. Chem. Phys.*, 2002, **117**, 8694–8704.
79 S. S. Iyengar, H. B. Schlegel, J. M. Millam, G. A. Voth, G. E. Scuseria and M. J. Frisch, *J. Chem. Phys.*, 2001, **115**, 10291–10302.
80 P. J. Hay and W. R. Wadt, *J. Chem. Phys.*, 1985, **82**, 299–310.